

Metallic foam processing from the liquid state

The competition between solidification and drainage

S.J. Cox^a, G. Bradley, and D. Weaire

Department of Physics, Trinity College, Dublin 2, Ireland

Received: 20 September 2000 / Revised and Accepted: 29 January 2001

Abstract. A model is developed to describe the formation of metallic foams in which liquid drainage acts to collapse the foam before it can freeze. Numerical solution of the foam drainage equation, combined with the equations of heat conduction, provides new insight into the competition between these two processes. It also stimulates and confirms a theoretical analysis which leads to criteria for creating uniform samples of frozen metal foam. The analysis suggests new experiments to clarify the role of the various processes leading to foam formation.

PACS. 82.70.Rr Aerosols and foams – 47.55.Mh Flows through porous media – 72.15.Cz Electrical and thermal conduction in amorphous and liquid metals and alloys

1 Introduction

In recent years, various techniques have been developed for the fabrication of metallic foams [1,2]. These remarkable materials have a structure that is broadly similar to the more familiar polyurethane foams, so that it may be described and analysed by the standard methods of foam science [3,4]. The mechanical properties of the constituent metal make the metallic foam relatively stiff and excellent for energy absorption. Applications in automobile manufacture are under development. Examples of metallic foams are shown in Figure 1.

While now well advanced, the technology of metallic foam formation still poses challenges. The solidification by cooling of a foamed liquid metal is a “race against time”, in as much as the relatively heavy and inviscid liquid is prone to drainage, which rapidly reduces the foam density and hence provokes instability and collapse. In this paper, we analyse the competition between drainage and heat transfer, leading to solidification, using an elementary model for computation.

The present analysis is one-dimensional: physically, this requires that heat is extracted only at the top and bottom surfaces of the sample. While this departs considerably from the usual experimental situation, we believe that there is much to be learned, in both a qualitative and semi-quantitative sense, from such a model. Furthermore, this model can be extended to three dimensions in due course. It may also be possible to test it directly with modified experiments in which the sides of the sample are insulated.

1.1 The process of foam formation

In the method used by Baumgärtner *et al.* [5] and others, a powdered metal is mixed with a blowing agent, pressed, and heated to its melting point. A blowing agent is chosen which releases gas close to this temperature, so that melting is accompanied by foaming. The sample is immediately cooled to trap this foam structure in a solid, closed-cell foam. (Other techniques may result in open-cell structures.) While the density of the foamed liquid may be considered to be initially uniform, it is immediately subjected to gravity-driven drainage of liquid, creating a vertical profile of density (or liquid fraction). At any point in the sample this adjustment must proceed until the freezing point is reached. Thus, at intermediate times, the sample consists of a solidified outer shell surrounding a draining liquid core.

1.2 Heat transfer, drainage and collapse

In developing a one-dimensional model of these competing processes, we shall make the simplest assumptions which capture the essential features of the problem. These relate properties to the local mean bubble diameter, D , and the relative density. This latter quantity is equivalent to the liquid fraction Φ_1 of a molten foam; however, when the foam solidifies we shall use the term *relative density*.

Firstly, it is assumed that solid/liquid conduction is the dominant mechanism of heat transfer. This contrasts with the case of insulating foams, in which the conduction of gas is dominant. We do not distinguish between solid and liquid conduction, so that the thermal conductivity of

^a e-mail: coxs@tcd.ie

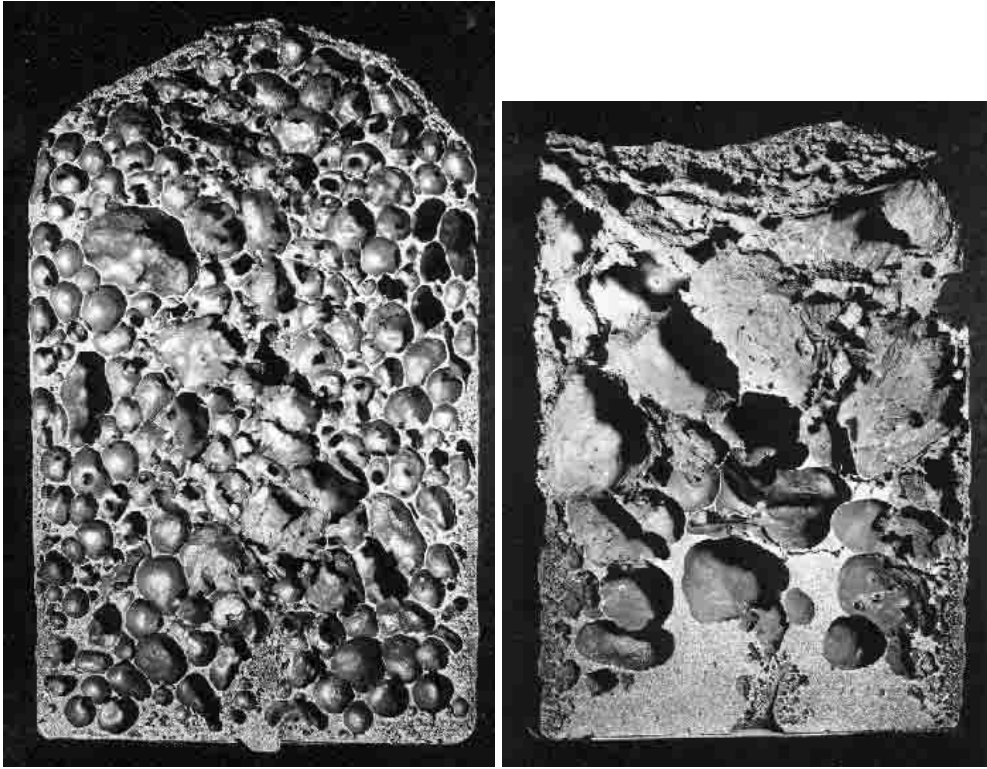


Fig. 1. The photographs show cross-sections through samples of foamed aluminium; the only difference is that the sample on the right has been kept in the furnace for a longer time. The foam on the left is well-formed, with uniform bubble size. However in the right-hand sample some of the bubbles have collapsed, others have coalesced, and significant drainage has occurred, leading to a large variation in bubble size as well as regions of solid metal. Both pictures are courtesy of J. Banhart and reproduced from I. Duarte and J. Banhart, *Acta Mater.* **48**, 2349 (2000).

the foam is directly proportional to Φ_1 and has the same coefficient in both phases.

The heat which is extracted is primarily the latent heat of freezing L_f , although we do include the relatively small heat capacity of solid and liquid, C_p . The latent heat is represented in the simulation by a finite spike in the specific heat capacity at the freezing temperature T_{crit} , purely as a matter of convenience.

Drainage is described by the Foam Drainage Equation [4,6–8], which is now well established (although some variation may be required in certain cases and can be accounted for in terms of surface viscosity [9,10]). This partial differential equation governs the variation of Φ_1 due to drainage of the Plateau borders (the liquid-filled channels between the bubbles) in the foam. It has not yet been specifically tested for metallic foams. A key parameter in the equation is the liquid viscosity, η , which we take to be a continuous function of temperature which rises to a very high value at the freezing point. Naturally, the actual variation of the viscosity is more complicated, especially for alloys, but this should capture its essential features.

Finally, we introduce a rule which allows for the rupture of thin films. This coalescence criterion is the most debatable ingredient of the model, and we would not make strong claims for its validity at this stage. For a more detailed discussion of the dynamics of film rupture, in the context of glass foam formation, see [11]. The

rationalisation of this rule is given in Section 2.1: its effect, in practice, is to prevent the size of the Plateau borders falling below a prescribed critical value anywhere. If the trend of drainage is towards a lower value at any point then the bubble diameter D at this point is increased, to simulate bubble coalescence. A compensating change of Φ_1 is then required by mass conservation, so that film rupture increases mean bubble size.

2 Mathematical formulation

In this section we give the details of the relevant equations for the processes of drainage and heat flux and describe how they interrelate. The results follow in Section 3, which should be readily understood in general terms without recourse to these details. The most important ingredients are the scheme used to represent the latent heat, and the viscosity equation which accounts for solidification in a simple way.

2.1 Drainage

The foam drainage equation is described elsewhere [12]; we briefly review its key elements here and demonstrate a slightly different non-dimensionalisation to be consistent

with the equations describing the heat flow and the viscosity.

The main assumption in deriving the drainage equation is that the contribution to drainage from the films is negligible, so that flow proceeds only through the Plateau borders. Consider first a single Plateau border, which need not be vertical, with cross-sectional area A that depends upon both the downward vertical coordinate z and time t . We define a parameter $N(z)$ which specifies the number of Plateau borders crossing a horizontal plane through the foam at height z . This allows us to relate the liquid fraction to the Plateau border area: $\Phi_1 = NA$. It also relates to the number of bubbles in any cross-section of the foam and will therefore help us to specify $D(z, t)$. However, the exact relationship between N , Φ_1 , D and the number of bubbles depends on the packing arrangement assumed for the foam.

The continuity equation for fluid, which is assumed to be incompressible, is

$$\frac{\partial(NA)}{\partial t} + \frac{\partial(NAu)}{\partial z} = 0 \quad (1)$$

where drainage theory gives the fluid velocity

$$u = \frac{\rho g A}{3f\eta} - \frac{C\gamma}{3f\eta} \frac{1}{2\sqrt{A}} \frac{\partial A}{\partial z}, \quad (2)$$

which is an average over the cross-section of the border and all its possible orientations. The combination of (1) and (2) gives the nonlinear partial differential equation for A or Φ_1 , which has become known as the Foam Drainage Equation. The viscosity is η , which will depend on temperature, ρ is the liquid density, g is the acceleration due to gravity, γ is surface tension and C and f are known geometrical factors. The liquid flow rate through each border is then $Q_1 = uA$. In steady drainage, where a uniform supply of liquid is added to the top of a foam, the foam drainage equation has the trivial solution that A is constant.

2.2 Heat

The heat flow due to conduction in a static foam is

$$Q_h = -\kappa \frac{\partial T}{\partial z}, \quad (3)$$

where $T(z, t)$ is the temperature and κ is the thermal conductivity. Then, using the substantial derivative, conservation of energy requires that

$$\rho\Phi_1 C_p \frac{DT}{Dt} = -\frac{\partial Q_h}{\partial z} \quad (4)$$

which becomes, using (3),

$$\rho\Phi_1 C_p \left(\frac{\partial T}{\partial t} + u \frac{\partial T}{\partial z} \right) = \frac{\partial}{\partial z} \left(\kappa \frac{\partial T}{\partial z} \right). \quad (5)$$

The specific heat is C_p , which we will make temperature dependent to conveniently account for the extraction of latent heat.

2.3 Non-dimensionalisation

We define the dimensionless variables $\tau, \xi, \alpha, \Theta, \hat{Q}_1, \hat{\eta}, \hat{\rho}, \hat{g}, \hat{C}_p$ and $\hat{\kappa}$ according to:

$$\begin{aligned} \text{time } t &= \tau t_0, \\ \text{position } z &= \xi z_0, \\ \text{plateau border area } A &= \alpha z_0^2, \\ \text{temperature } T &= \Theta (T_{\text{init}} - T_0) + T_0, \\ \text{liquid flow rate } Q_1 &= \hat{Q}_1 Q_1^0, \\ \text{liquid viscosity } \eta &= \hat{\eta} \eta_0, \\ \text{liquid density } \rho &= \hat{\rho} \rho_0, \\ \text{gravity } g &= \hat{g} g_0, \\ \text{specific heat } C_p &= \hat{C}_p C_p^0, \\ \text{thermal conductivity } \kappa &= \hat{\kappa} \kappa_0 \Phi_1 \end{aligned}$$

in which

$$t_0 = \frac{3f\eta_0}{\sqrt{C\gamma\rho_0g_0}}, \quad z_0 = \sqrt{\frac{C\gamma}{\rho_0g_0}} \quad \text{and} \quad Q_1^0 = \frac{C^2\gamma^2}{3f\eta_0\rho_0g_0}.$$

T_{init} is the initial temperature of the foam, T_0 the cooling temperature, $g_0 = 9.8 \text{ m/s}^2$ and ρ_0, η_0, C_p^0 and κ_0 will depend on the particular metal being foamed. Note that κ is scaled by Φ_1 , so that a denser foam transports more heat.

The dimensionless equations which must then be solved simultaneously are those of liquid drainage:

$$\frac{\partial(N\alpha)}{\partial \tau} + \frac{\partial(N\hat{Q}_1)}{\partial \xi} = 0, \quad (6)$$

in which the liquid flow rate is

$$\hat{Q}_1 = \frac{1}{\hat{\eta}} \left(\hat{\rho} \hat{g} \alpha^2 - \frac{\sqrt{\alpha}}{2} \frac{\partial \alpha}{\partial \xi} \right), \quad (7)$$

and heat flow:

$$\hat{\rho} \hat{\Phi}_1 \hat{C}_p \left(\frac{\partial \Theta}{\partial \tau} + \frac{\hat{Q}_1}{\alpha} \frac{\partial \Theta}{\partial \xi} \right) = \frac{1}{Pe} \frac{\partial}{\partial \xi} \left(\hat{\kappa} \hat{\Phi}_1 \frac{\partial \Theta}{\partial \xi} \right), \quad (8)$$

where the Peclet number is

$$Pe = \frac{z_0^2 \rho_0 C_p^0}{t_0 \kappa_0}. \quad (9)$$

Since neither the liquid density or thermal conductivity will change, we can equate both $\hat{\kappa}$ and $\hat{\rho}$ with unity. We expect Pe to be of order unity, giving approximately equal weighting to the advection and conduction terms.

2.4 Viscosity and latent heat

To describe a foam in both its solid and liquid states, we choose a smooth step function for the dimensional viscosity η that gives small values η_0 at high temperatures and

high values η_{\max} at low temperatures when the foam is frozen. We write

$$\hat{\eta} = 1 + \frac{\eta_{\max}/\eta_0 - 1}{1 + \exp(w_\eta(\Theta - \Theta_{\text{crit}}))}. \quad (10)$$

The value of η_{\max}/η_0 must be sufficiently high that there is no drainage at the low temperatures at which the foam is effectively solid. The parameter w_η measures the narrow range of temperature over which the viscosity changes from η_0 to η_{\max} . This ‘‘mushy’’ zone is in practice achieved by the use of metal alloys; it may be that in a less basic model than this the precise details of the change in viscosity must be taken into account. In what follows, we consistently use the values $\eta_{\max}/\eta_0 = 10^5$ and $w_\eta = 10^4$; the precise values of these two parameters are not significant.

To incorporate the latent heat of fusion, we change the specific heat to

$$\hat{C}_p = 1 + \frac{L_f w}{C_p^0 \sqrt{\pi}} \exp\left[-(w(\Theta - \Theta_{\text{crit}}))^2\right]. \quad (11)$$

This describes a symmetrical peak in the specific heat, around the melting temperature, which represents the heat that must be absorbed before the foam solidifies; this is purely a convenient way of representing L_f . The parameter w measures the range in temperature of the peak (and is different to w_η). We will retain $w = 50$ throughout and normalise the latent heat by C_p^0 ; that is, $L_f \rightarrow L_f/C_p^0$. We take $L_f = 10$.

2.5 Boundary conditions

We impose boundary conditions of no flow ($\hat{Q}_1 = 0$) at the top ($\xi = 0$), since no fluid enters the system, and at the bottom ($\xi = L$), where the foam is being cooled. Note that if $\hat{Q}_1 = 0$ is specified everywhere, then we obtain the *equilibrium profile* of the foam:

$$\alpha_{\text{eq}}(\xi) = \left(\frac{1}{\sqrt{\alpha_L}} + L - \xi\right)^{-2} \quad (12)$$

where α_L corresponds to the liquid fraction at the bottom of the foam. This is the profile to which all liquid foams are eventually brought by gravity drainage; note that α_{eq} is nowhere zero.

The boundary conditions associated with the temperature are that the bulk of the foam is initially at uniform temperature $T = T_{\text{init}} \Rightarrow \Theta = 1$ while the lower end has $T = T_0 \Rightarrow \Theta = 0$. The freezing temperature translates into a value Θ_{crit} between zero and one. We take $\Theta_{\text{crit}} = 0.9$ throughout.

We consider two scenarios for the top temperature condition (see Fig. 2): case I, where the sample is cooled in the same way as the bottom, with the condition $\Theta = 0$, and case II, where the top boundary condition is that of no heat flow, $\partial\Theta/\partial\xi = 0$, so that cooling proceeds only from the bottom.

We assume that the number of borders N is initially uniform throughout the sample. In the model described here, N changes only by virtue of coalescence. We hypothesise that films will rupture below a critical thickness, and since the equilibrium film thickness should be a monotonic function of the Plateau border area, we allow bubbles to merge when this area becomes smaller than some critical value, $\alpha < \alpha_{\text{crit}}$. At this point ξ_1 we decrease $N(\xi_1)$ to

$$N(\xi_1)\alpha(\xi_1, \tau)/\alpha_{\text{crit}}$$

then put $\alpha(\xi_1, \tau) = \alpha_{\text{crit}}$ so that D increases accordingly. (In the event of coalescence, we will assume that the change is small enough that we can ignore the temporal derivative of N in (1).) We will assume throughout an initial distribution of $N(\xi) = 1 \quad \forall \xi$ to simplify the analysis.

The liquid fraction of the foam is given by $\Phi_1 = N\alpha$. If each bubble has a cross-sectional area of $\pi(D/2)^2$ we have that

$$D(\xi, \tau) = 2\sqrt{\frac{1 - \Phi_1}{N\pi}}. \quad (13)$$

Therefore D is also initially constant, but will subsequently change as Φ_1 varies and as bubbles coalesce.

2.6 Method of solution

We solve (6) and (8) using an explicit finite difference representation with constant step sizes in both time (upwind) and space. This conservative formulation minimises errors due to numerical roundoff.

We now retain all variables in dimensionless form, but omit their caps, *e.g.* $\hat{\rho} \rightarrow \rho$.

3 Results

We shall describe in detail only the progress of solidification for case I, since case II is in some sense equivalent to the lower half of the sample in case I. In this case two freezing fronts move inwards to meet near the centre of the sample. Behind each front there is an approximately linear variation of relative density. In the next part we describe the results of numerical simulations. These provide the motivation for an analytic model, detailed in Section 3.2, which compares well with the full solution. Sections 3.3 and 3.4 describe various extensions to the model, including the coalescence criterion and the effects of varying the gravitational acceleration.

3.1 Examples

We show in Figures 3 and 4 how the profile of Φ_1 evolves over time. In both cases the liquid fraction is initially uniform, that is, it is represented by a vertical line $\Phi_1 = \Phi_1^0$. In case I (Fig. 3) both ends are frozen at time $\tau = 0$. The

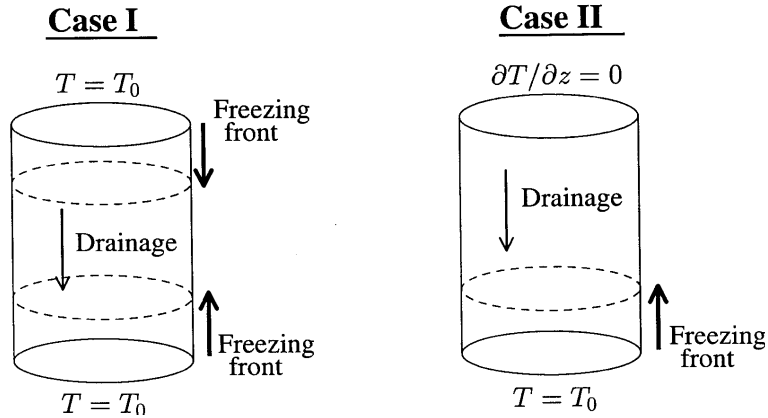


Fig. 2. A sketch of the two cases considered, showing the competition between drainage and freezing.

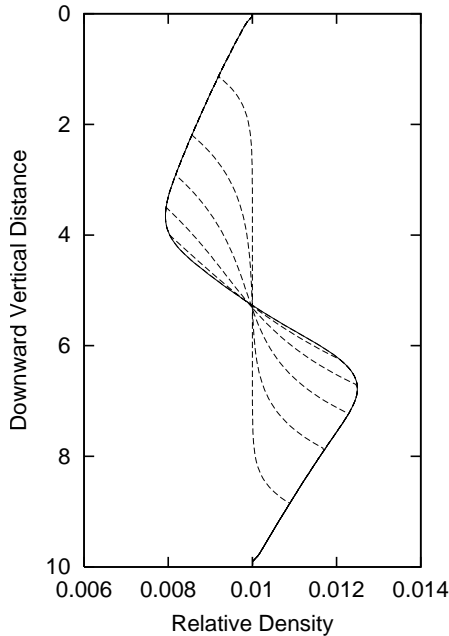


Fig. 3. Successive profiles of relative density are shown for case I, starting from a liquid foam with constant liquid fraction $\Phi_1^0 = 0.01$ and $Pe = 1$. Dashed lines denote the profiles at time intervals of $\tau = 20$ and the solid line is the eventual, frozen, profile at $\tau = 140$.

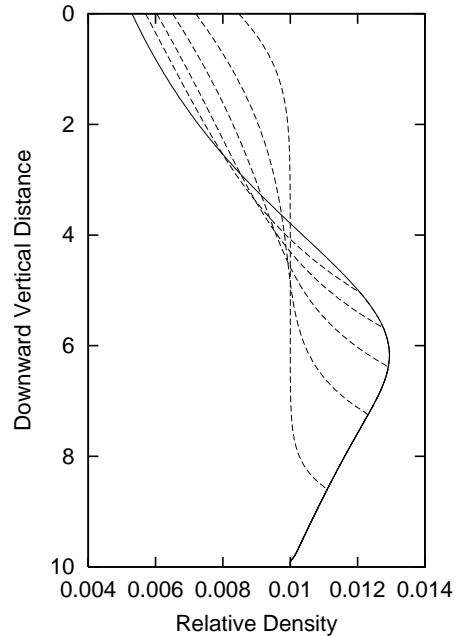


Fig. 4. Successive profiles of relative density are shown for case II, starting from a liquid foam with constant liquid fraction $\Phi_1^0 = 0.01$ and $Pe = 1$. Dashed lines denote the profiles at time intervals of $\tau = 36$ and the solid line is the eventual frozen profile at $\tau = 450$.

relative density at the top of the foam initially decreases as liquid drains due to gravity, and the freezing front also moves downward, towards the centre of the foam, to give an approximately linear decrease in relative density in the frozen sample.

At the bottom of the foam a freezing front moves upward. At the same time, liquid drains towards this front, and accumulates above it before being frozen itself. Therefore the relative density at the bottom of the foam grows, and again this increase in Φ_1 is roughly linear, with a similar slope to the one at the top of the sample.

The relative density between the two freezing fronts, in the centre of the foam, at first remains close to its initial

value, but in due course it evolves towards a profile which smoothly interpolates between the low values of Φ_1 at the top of the foam and the high values at the bottom. In the final phase of its evolution, the profile of this central region, which is still liquid, closely approaches the equilibrium form (12). It therefore ceases to change appreciably as the two freezing fronts proceed to meet and solidify the entire sample. This can be seen in the profiles for case I in Figure 3, but is even clearer in Figure 4: in case II there is a greater proportion of the sample which is molten, yet the profile at time $\tau = 216$ is indistinguishable from the final profile at $\tau = 450$.

In case II, the liquid fraction at the top of the foam decreases just as it would in the standard free drainage experiment [12], until it is frozen at the very end of the process when the freezing front reaches the top.

So in case I the characteristic form of the final profile is that of a “sawtooth” pattern. This resulting variation in relative density is generally undesirable. The theory which we next elucidate, in Section 3.2, offers a criterion for the avoidance of such inhomogeneity in terms of the physical parameters and the sample dimensions.

3.2 Analytic approximation

The linearity of the profiles of relative density at the top and bottom of the foam suggests that it may be possible to supply an analytical description of the early stages of the solidification process. We now try to reproduce the early evolution of the profile with a simple theory which appeals to conservation of both heat and liquid. The first step is to find the distance of the freezing fronts from the top and bottom of the sample, as a function of time. Then the quantity of liquid which has drained in this time is calculated, to enable the variation of relative density to be found.

To find the position of the freezing front, we consider the heat loss from the top of the foam in unit time. On the one hand, (3) shows that the heat flux Q_h varies as $\kappa(T_{\text{crit}} - T_0)/x_f$, where x_f is the distance of the front from the top of the foam. But the amount of heat extracted in unit time is equal to the product of the latent heat, the velocity of the front and the mass of liquid: $L_f \rho \Phi_1 dx_f/dt$, ignoring the contribution of the specific heat. Thus, in the dimensionless variables used here,

$$L_f \rho \Phi_1 \frac{d\xi_f}{d\tau} = \frac{\kappa \Phi_1 \Theta_{\text{crit}}}{Pe \xi_f}. \quad (14)$$

Integrating (14) gives

$$\xi_f^2 = \frac{2\kappa \Theta_{\text{crit}}}{Pe L_f \rho} \tau, \quad (15)$$

enabling the position of the front to be found as a function of time. At the bottom of the sample the same argument is applicable, with ξ_f replaced by $L - \xi_f$, so that in Figure 5 we can compare the position of the fronts at both the top and the bottom of the foam.

It is possible to track the position of the freezing fronts using our numerical code, so that we can estimate the accuracy of (15) in comparison with the full model. The agreement, also shown in Figure 5, is excellent. The freezing front moving up the foam in case II has much the same shape but continues to ascend.

Now, to continue in our stated aim of recreating the final profile of relative density, we must consider a balance of mass transport. The volume of fluid drained from the top of the sample is approximately equal to the area of the growing triangles sketched in Figure 6, based upon the neglect of the diffusive, or smoothing, term in the liquid flow rate. This area is $V = \frac{1}{2} x_f^2 (-d\Phi_1/dx)$.

At early times, the central part of the profile has constant liquid fraction and therefore constant flow rate. Further, the liquid that has drained from the top of the sample must pass through this region. So this volume of liquid is equal to the product of the flow rate and time: $V = N Q_1 \tau$. Thus

$$\frac{1}{2} \xi_f^2 \left(-\frac{d\Phi_1}{d\xi} \right) = N Q_1 \tau. \quad (16)$$

We can then substitute for ξ_f from (15), to give not only the slope of the relative density at the top of the foam:

$$\frac{d\Phi_1}{d\xi} = -\frac{Pe N L_f \rho \rho g (\Phi_1^0)^2}{\kappa \Theta_{\text{crit}} N^2 \eta_0} = -\frac{Pe L_f \rho^2 g (\Phi_1^0)^2}{N \kappa \Theta_{\text{crit}} \eta_0} \quad (17)$$

but also, upon integration, the variation of the relative density itself:

$$\Phi_1 = \Phi_1^0 - \frac{Pe L_f \rho^2 g (\Phi_1^0)^2}{N \kappa \Theta_{\text{crit}} \eta_0} \xi. \quad (18)$$

Can we apply the same argument at the bottom of the foam to give the same slope of relative density? We appeal to conservation of liquid (the bottom of the sample is initially frozen so that no liquid can escape) and note that the freezing front moving up from the bottom has the same speed as the descending front, in the absence of heat transport due to drainage. Then a similar derivation to the above gives

$$\Phi_1 = \Phi_1^0 + \frac{Pe L_f \rho^2 g (\Phi_1^0)^2}{N \kappa \Theta_{\text{crit}} \eta_0} (L - \xi) \quad (19)$$

so that the ends of the final profile are antisymmetric.

An approximation to the central part of the final profile is somewhat more straightforward to calculate. As noted earlier, the sample stops draining before it is everywhere frozen. Therefore gravity drainage must be the dominant process in the central region, so we expect that the eventual profile in the middle of the foam will closely approach the equilibrium profile (12). The particular profile connecting the two linear segments is given uniquely by the central point of the initial profile of phase fraction: that is, we substitute $\alpha_L = \Phi_1^0/N$ and replace L by $L/2$ in (12):

$$\Phi_1 = \left(\sqrt{\frac{N}{\Phi_1^0}} + \frac{L}{2} - \xi \right)^{-2}. \quad (20)$$

To complete the final profile of relative density we must join the two straight end sections to the central “equilibrium” section. To find each of the points of intersection requires the solution of a cubic equation for ξ , given by equating (20) with (18) and with (19) respectively. In the case illustrated in Figure 7 we find $\xi = 2.9$ and $\xi = 6.5$. Resubstitution gives a minimum value of $\Phi_1 = 0.007$ and a maximum of $\Phi_1 = 0.014$.

It should be noted that this formulation incorporates a small but finite change in the total volume of liquid present

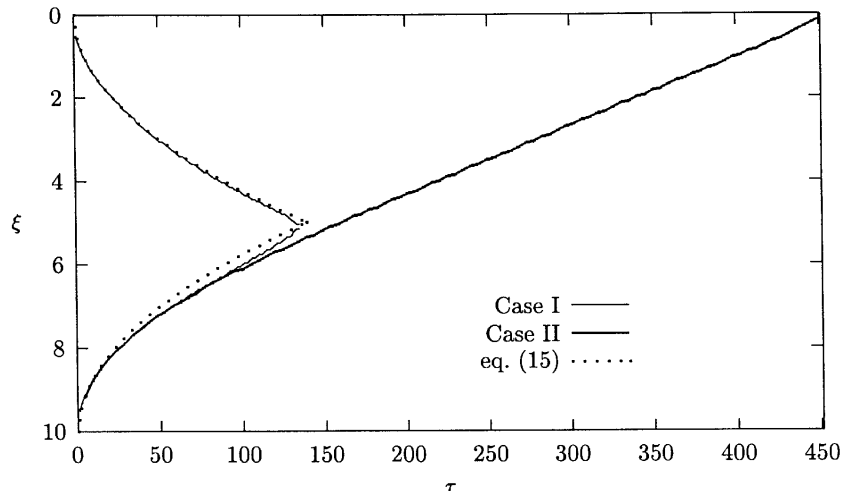


Fig. 5. The position ξ of the freezing fronts against time τ in both cases, for the profiles shown in Figures 3 and 4. Also shown is the analytical result (15), for both the top and bottom fronts. This result is an excellent approximation at the top of the foam. We attribute the small discrepancy at the bottom to the neglect of the specific heat and the contribution of drainage to reduced cooling in the lower part of the foam.

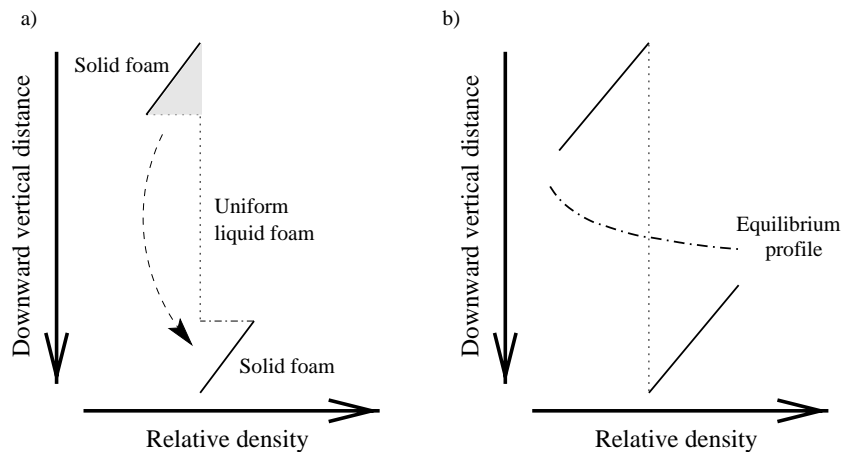


Fig. 6. A description of the approximations made in reproducing the profiles of relative density analytically for case I. (a) At early times, the relative density at the top decreases linearly, and at the bottom it increases linearly, with the same slope. The centre of the profile remains at its initial, constant, value (the dotted line). The area of the shaded triangle represents the volume of fluid which has drained down to the bottom of the foam. (b) At much later times, when the foam is frozen, the linear regimes have extended farther towards the centre of the foam. These two sections are joined by a smooth “equilibrium” curve.

(approximately one percent for the calculation shown); in practice this is corrected by the lack of antisymmetry in the end profiles, which also shifts the central section downwards.

In Figure 7 we compare these approximate profiles with the full numerical solution. Given that we have neglected the specific heat, the agreement is remarkably good. These estimates could be improved further with a more accurate estimation of the volume of liquid which has drained from the top of the foam, since the overestimate in the slope is due to an underestimate in calculating the triangle area.

The volume flux balance (17) describing the variation of the slope of relative density with position suggests a

criterion for deciding when a metallic foam sample will be uniform/homogeneous. This would require a small value of

$$\frac{L}{\Phi_1} \frac{d\Phi_1}{d\xi}.$$

Then we suggest the following

$$\text{homogeneity criterion: } \frac{PeL_f \rho^2 g L \Phi_1^0}{N \kappa \Theta_{\text{crit}} \eta_0} \ll 1. \quad (21)$$

For the parameter values used here ($L_f = 10$, $\Theta_{\text{crit}} = 0.9$, $L = 10$, $\rho = g = \kappa_0 = \eta_0 = N = 1$ and $\Phi_1 = 0.01$) this quantity is slightly greater than one; the results in Figure 7 show that the maximum deviation from homogeneity is about 40% of the initial liquid fraction.

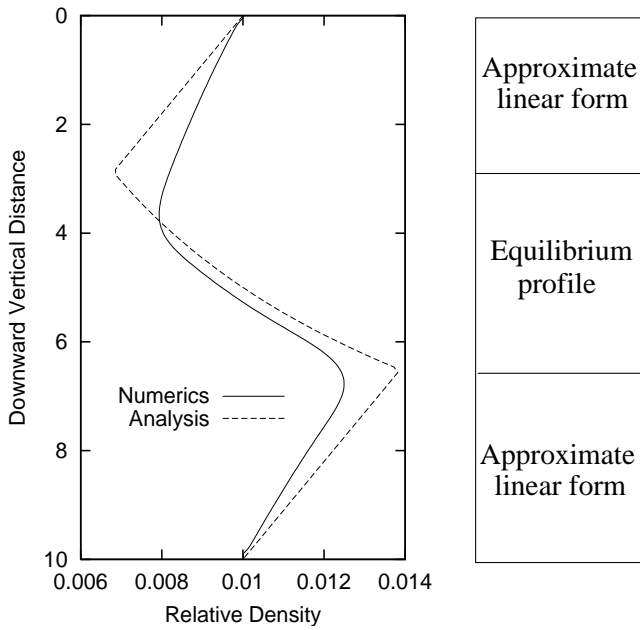


Fig. 7. Comparison between theory and numerics in case I. The final profile of phase fraction is redrawn from Figure 3, to show how good the analytic result is. The straight sections are given by (18) and (19), and are joined uniquely by a section of the equilibrium solution (12). The differences are due mostly to the error in approximating the amount of liquid drained (triangle area), and also to the neglect of the specific heat.

Variation of freezing time

We should supplement this criterion with a measure of the total freezing time, τ_f . That is, how long does it take for the whole sample to freeze? Note that the sample may stop draining, and reach equilibrium under gravity, *before* it is everywhere solid.

We refer again to (15); the length of foam which must be frozen is $L/2$, so that

$$\tau_f = \frac{PeL_f\rho L^2}{8\kappa\Theta_{crit}}. \quad (22)$$

This gives $\tau_f = 139$ in case I, while our computations give $\tau_f = 133$, and in general further results of numerical calculation show good agreement with this functional for t_f . So, as would be expected in any heat diffusion problem, the freezing time is proportional to the square of the length of the foam, and in inverse proportion to the thermal conductivity.

3.3 Coalescence and collapse

When the criterion (21) for homogeneity is not satisfied, we expect additional effects. In particular, the bubbles of the foam will coalesce where the liquid fraction is small and a liquid pool will form where the liquid fraction becomes large. Any one of several changes in the physical

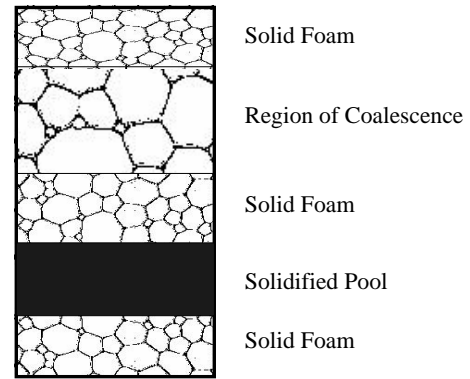


Fig. 8. If the initial value of Φ_1^0 is increased tenfold, we enter the strongly inhomogeneous regime, as illustrated schematically. Our simulations show that coalescence occurs near the top of the foam, where the relative density falls, and a liquid pool forms near the bottom of the foam. This pool will freeze in due course to form a lump of solid metal. (The bubble structure is purely for illustrative purposes, and does not represent the result of the calculations described here.)

parameters or dimensions of the foam may cause these events to occur; in Figure 8 we sketch the effect of a higher initial liquid fraction. An increase in the initial liquid fraction Φ_1^0 also changes the shape of the lower freezing front, so that its central part becomes linear. This is due to the dependence of the thermal conductivity on Φ_1 .

In case II we would expect coalescence to occur in the same way, but at the very top of the foam.

Although our numerical code breaks down with the formation of a pool, because there are no longer bubbles present, we can use it to investigate coalescence using the model described in Section 2.5. That is, we introduce a cut-off at low Plateau border areas α , at which point we allow the number of bubbles N to increase. The results are shown in Figure 9, which displays the bubble size distribution for the profiles of Figure 3 with a coalescence criterion of $\alpha_{crit} = 0.9\Phi_1^0$. Without assuming a particular bubble packing, however, this measure of D may be taken as a guide only. The figure does show that bubble size can increase significantly. We find also that the profile of liquid fraction is shifted upward and freezing times are lengthened slightly, since the “velocity” of heat conduction is reduced in this bubbly region of the foam.

3.4 Microgravity

Variation of the parameter g allows the model to be used to predict the effect of metallic foam formation in space or in parabolic flights. A decrease in gravity to around $g = 0.001$, for example, changes the criterion for homogeneity (21) by three orders of magnitude, since it slows down drainage. Thus, as expected, our model predicts that it will much easier to make metallic foams with uniform relative density in space, all other parameters being equal.

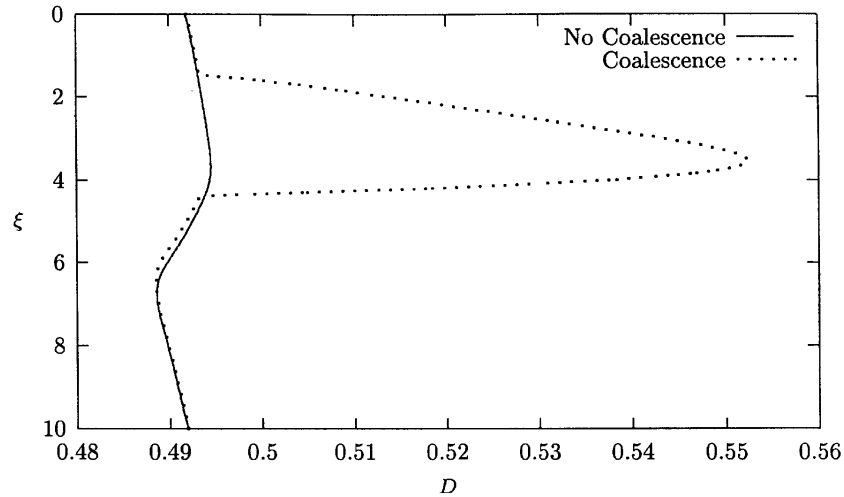


Fig. 9. Demonstrating the effect on the bubble diameter, D (in arbitrary units), of introducing a coalescence criterion in case I. There is a small variation in D because of the change in liquid fraction due to drainage, but the large peak is due to bubbles merging when the walls between them become too thin. The initial liquid fraction is $\Phi_1^0 = 0.01$ and $Pe = 1$.

4 Summary

The development of metallic foam is proceeding apace, while the theoretical description of its formation lags well behind. We have supplied a first description of the freezing stage of this formation process, using a one-dimensional model which combines the equations of foam drainage with those of conductive heat transfer.

Comparisons between our numerical results and a simple analytic theory are very encouraging. The numerics include the effects of coalescence, indicating where metallic foams may contain gaps, and also where the foam itself may collapse. The theoretical approximations work best in the limit of low liquid fraction, *i.e.* for dry foams, which is also the limit in which the foam drainage equation is best applied.

Moreover, the theory allows us to specify a criterion for homogeneity of the final, solid, foam (21) in terms of the physical parameters of the constituent metal and the dimensions of the sample. In combination with this criterion, we give a sketch in Figure 10 of the interaction between some of the more easily adjustable parameters. We suggest that collapse is more likely to occur in long or wet foams where the liquid metal is heated to well above the melting point.

We believe that comparison with one-dimensional experiments, yet to be performed, would be extremely useful for the development of this theory. The extraction of heat from only the top and bottom of the sample is currently an idealisation, but we have shown that it allows clear and concise analysis of the process.

In extending the method to three dimensions, we foresee few difficulties. The important extensions will be to improve our coding of film rupture/coalescence and liquid collection.

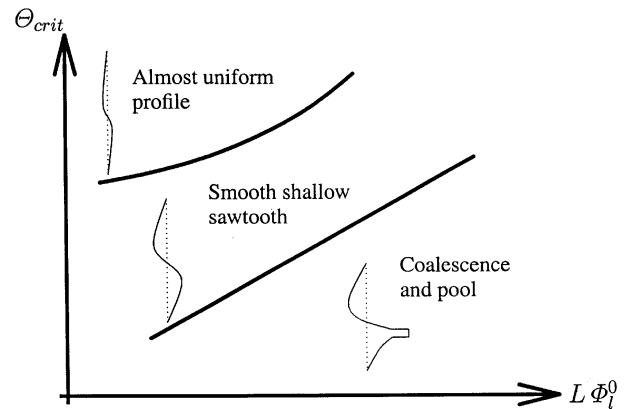


Fig. 10. The variation of the final profile of relative density, in case I, with the product of the length of the foam L and its initial liquid fraction, and the melting point of the molten metal Θ_{crit} . The small inset sketches suggest possible final profiles of position against relative density. As Θ_{crit} decreases, the point of maximum relative density in the final profile moves toward the bottom of the foam. As L or Φ_1^0 increases, the maximum relative density grows. Both of these scenarios are likely to lead to foam collapse, due to coarsening and liquid accumulation.

The authors wish to thank J. Banhart, P. Yecko, G. Verbist and T. Wübben for useful discussions, and the referees for useful comments and suggestions for further work. This research was supported by the Prodex programme of ESA, and is a contribution to ESA contract C14308/AO-075-99. SJC was supported by Enterprise Ireland and a Marie Curie fellowship. GB was supported by the HPC Programme of TCD.

Appendix: Notation

$A(z, t), \alpha(\xi, \tau)$	Plateau border area
$C^2 = \sqrt{3} - \pi/2$	Geometrical constant associated with Plateau border
C_p	Generalised specific heat capacity
γ	Surface tension
$D(\xi, \tau)$	Gas bubble diameter
$f \approx 50$	Constant for Poiseuille flow in Plateau border
g	Acceleration due to gravity
$\kappa(\Phi_1)$	Thermal conductivity
L_f	Latent heat of fusion
η	Viscosity
$N(\xi)$	Number of Plateau borders crossing a unit area of foam
Pe	Peclet number
Φ_1	Relative density or liquid fraction of foam
ρ	Liquid density
$Q_h(\xi, \tau)$	Heat flow rate
$Q_l(\xi, \tau)$	Liquid flow rate
t, τ	Time
τ_f	Dimensionless time at which foam completely solidified
$T(z, t), \Theta(\xi, \tau)$	Temperature
u	Liquid flow velocity
V	Volume of drained fluid
z, ξ	Position in foam $0 \leq \xi \leq L$

References

1. M.F. Ashby, A.G. Evans, N.A. Fleck, L.J. Gibson, J.W. Hutchinson, H.N.G. Wadley, *Metal Foams: A Design Guide* (Butterworth-Heinemann, Boston, 2000).
2. J. Banhart, in *Foams, Emulsions and Their Applications*, edited by P. Zitha, J. Banhart, G. Verbist (MIT-Verlag, Bremen, 2000), p. 13.
3. *Metal Foams and Porous Metal Structures*, edited by J. Banhart, M.F. Ashby, N.A. Fleck (MIT-Verlag, Bremen, 1999).
4. D. Weaire, S. Hutzler, *The Physics of Foams* (Clarendon Press, Oxford, 1999).
5. F. Baumgärtner, I. Duarte, J. Banhart, *Adv. Eng. Mat.* **2**, 168 (2000).
6. G. Verbist, D. Weaire, *Europhys. Lett.* **26**, 631 (1994).
7. G. Verbist, D. Weaire, A.M. Kraynik, *J. Phys.-Cond. Matter* **8**, 3715 (1996).
8. S.J. Cox, D. Weaire, S. Hutzler, J. Murphy, R. Phelan, G. Verbist, *Proc. Roy. Soc. London A* **456**, 2441 (2000).
9. S.A. Koehler, S. Hilgenfeldt, H.A. Stone, *Phys. Rev. Lett.* **82**, 4232 (1999).
10. M. Durand, G. Martinoty, D. Langevin, *Phys. Rev. E* **60**, R6307 (1999).
11. N. Pittet, in *Foams and Emulsions*, edited by S.F. Sadoc, N. Rivier (Nato Science Series: E Applied Sciences, Kluwer, Dordrecht, 1999).
12. D. Weaire, S. Hutzler, G. Verbist, E. Peters, *Adv. Chem. Phys.* **102**, 315 (1997).